Long-Lasting Electromagnetic Ion Cyclotron Waves Evident During Low Impact Geomagnetic Storms

By

Maeve Rodgers

Astrophysical and Planetary Sciences Department, University of Colorado Boulder

April 3^{rd}, 2024

Honors Council Representative:

Mark Rast, Astrophysical and Planetary Sciences

Defense Committee:

Lauren Blum, Astrophysical and Planetary Sciences (Thesis Advisor)

Bethany Wilcox, Physics (Outside Reader)

Seth Hornstein, Astrophysical and Planetary Sciences (Additional Committee Member)

Long-Lasting Electromagnetic Ion Cyclotron Waves Evident During Low Impact Geomagnetic Storms

Maeve Rodgers [*1] and Lauren Blum [†2]
[1] *University of Colorado Boulder, Boulder, Colorado*
[2] *Laboratory of Atmospheric and Space Physics, Boulder, Colorado*

Minor geomagnetic storms occur at a Dst (Disturbance Storm Time) rating of $\leq |-60|$ nT. While these low-intensity storms typically do not engender any disruptions to everyday life, an extensive examination of magnetic field data reveals the emergence of a discernible pattern. On multiple occasions, during minor geomagnetic (G1) storms, there have been instances of prolonged electromagnetic ion cyclotron (EMIC) waves. Normally, EMIC waves endure for a few minutes to an hour at most; however, recent observations indicate that these waves can persist at least five hours and on consecutive days. These long-duration EMIC events have sparked considerable interest as they exhibit uncharacteristic behavior not previously observed in EMIC waves. In this research endeavor we map the occurrences of these protracted EMIC waves across multiple days and events. By employing these maps, we can investigate the underlying causes for the unusually long-durations of these waves. Consequently, this analysis establishes a novel approach to mapping waves in the Earth's magnetosphere, while simultaneously providing an elucidation on the mechanisms responsible for enduring EMIC waves during low-intensity G1 storms.

I. Introduction

Electromagnetic ion cyclotron (EMIC) waves are plasma waves generated in the inner-magnetosphere by ring current ions and are typically registered on the ground in the Pc_{1-2} (0.1 to 5 Hz) frequency range (Usanova et al. 2008). EMIC waves can resonate with protons and high energy electrons, making them an important process for understanding the dynamics of multiple particle populations in the Earth's magnetosphere and are important in understanding proton precipitation, subauroral processes, electron disruptions, ring current and radiation belt dynamics (Wang et. al., 2015). Generally, we can expect EMIC waves to propagate in the day-side and dusk sector, as shown in Figure 1. Dayside waves are often caused by compressions or solar wind pressure increases, while duskside waves are generally more localized and generated by individual particle injections during substorm activity and geomagnetic storms (Blum et. al., 2015)

Low impact storms (G1 storms) generally occur when the magnetosphere is hit with a sustained high speed stream

[*]Research Assistant, Laboratory of Atmospheric and Space Physics, maeve.rodgers@colorado.edu
[†]Senior Researcher, Laboratory of Atmospheric and Space Physics

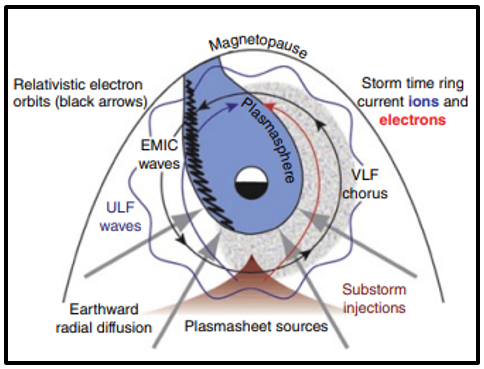

Fig. 1 Diagram showing EMIC location in magnetosphere (Usanova et al., 2016). The dayside is towards the top and the nightside is toward the bottom.

of solar wind. This causes a disturbance in the magnetic field around Earth resulting in energized particles that can interact causing waves to propagate through the magnetosphere.

Depending on what point in the solar cycle we are at, there are different causes for each storm we could be looking at. During the rising phase, we tend to see more solar flares and coronal mass ejections (CMEs) which send high speed, energized particles toward Earth. During the declining phase of the solar cycle, we tend to see more coronal holing and corotating interaction regions (CIRs) that cause high speed streams to impact Earth (Borovsky and Denton, 2006). It is known that relativistic electron flux is maximized during the declining phase and ultra low frequency (ULF) pulsations are longer duration during CIR-driven storms (Borovsky and Denton, 2006). The Earth's ring current is the current system responsible for observed worldwide decreases in the surface magnetic field (Williams, 1985). It is important to note that the ring current is weaker during CIR-driven storms and thus could appear as G1 storms on readings.

The spatial and temporal properties of EMIC waves have shown a dependence on wave properties, location, and generation mechanism (Blum et al., 2017). Multiple studies on dayside compression-driven EMIC activity have shown that this activity is most generally short-duration spanning across large spatial regions (e.g., Engebretson et al., 2018, Usanova et al., 2008). Generally, long-duration activity is contained on the dusk/nightside and caused during the recovery period of geomagnetic storms (Usanova, 2008, Blum 2020, Kakad 2023). The recovery period is the time after a geomagnetic storm that is characterized by and increase in the Dst back to 0 nT. During the main phase of a storm, the outer radiation belt electron flux rapidly dropped before subsequently becoming enhanced to levels greater than the pre-storm flux levels (Ozeke et. al., 2020). Preferential excitation of EMIC waves along the duskside is suggested as a possible explanation for rapid radiation belt flux dropouts that can occur during the main phase of geomagnetic storms (Usanova, 2008). Duskside and nightside EMIC waves often exhibit a more localized nature, commonly associated with discrete bursts of energetic particles during substorm activity. Within the inner magnetosphere's nightside, these waves persist during the recovery phase of a storm, coinciding with the presence of hot ions and the outward expansion of the plasmasphere across a broad range of local times (Blum et. al., 2020, 2024).

Local time, or LT, refers to the time observed in a particular geographical region or time zone. It is based on the position of the Sun relative to a specific location on Earth. It is important to recognize the LT of ground station data in order to determine an accurate location of the waves. Universal time, or UT, is the primary time standard by which the world regulates clocks and time. UT is the general metric for how magnetosphere data is labeled. Generally, databases will sort and store data using the UT in which it was recorded at. Then later, we can perform time conversions to learn the LT that an event occurred at, to better understand where in the magnetosphere it occurred (e.g. dayside or duskside).

For this study, we utilize Canadian Array for Realtime Investigations of Magnetic Activity (CARISMA) ground stations' magnetic field data to observe EMIC activity during low magnitude storms (Dst ≥ -60 nT) on the following dates: March 20th – 23rd, 2018 and July 17th – July 19th, 2020, to explore long duration wave activity. Furthermore, we explore solar wind conditions, geomagnetic activity, and plasma environment conditions using the OMNI dataset provided by NASA's Space Physics Data Facility (SPDF). In the following sections we provide CARISMA observations of EMIC activity as well as relative locations and timing of these measurements. The purpose of this study is to better determine the timing, duration, and drivers of the EMIC waves observed during these G1 storms that are either lasting multiple days or starting and stopping multiple times during the recovery phase of the storm.

II. Methodology

Wave observations presented in this paper are provided by the CARISMA magnetometers throughout Canada. CARISMA fluxgate magnetometers (FGMs) provide two components of the magnetic field at a cadence of up to 8 samples/second. The data we used was recorded at 1Hz and thus could be resolved up to .5Hz. The data from CARISMA is plotted daily between 0 and .5 Hz.

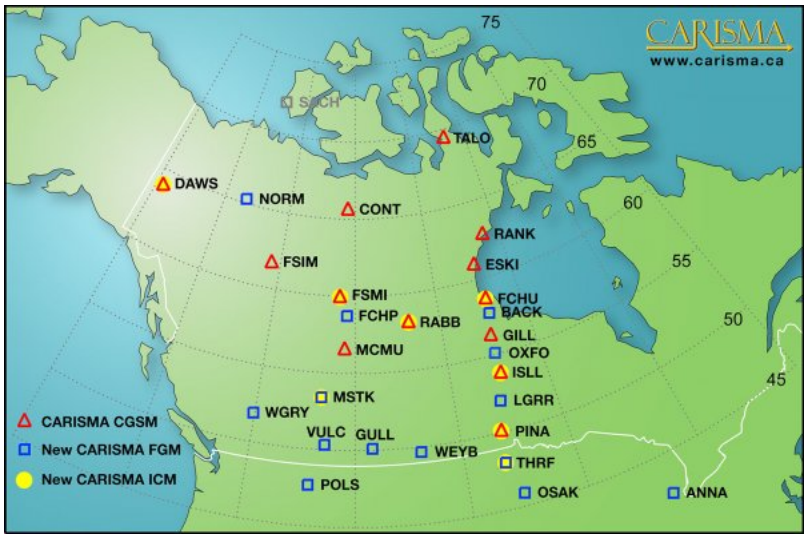

Fig. 2 CARISMA station locations across Canada

The World Data Center for Geomagnetism and Space Magnetism in Kyoto, Japan provides the Dst index for multiple years. Using this service, we found G1 storms of Dst $\leq |-60|$ nT on March 20th, 2018, and July 17th, 2020. Looking at the CARISMA data on these days, we observed hours-long EMIC wave activity on multiple consecutive days throughout both events.

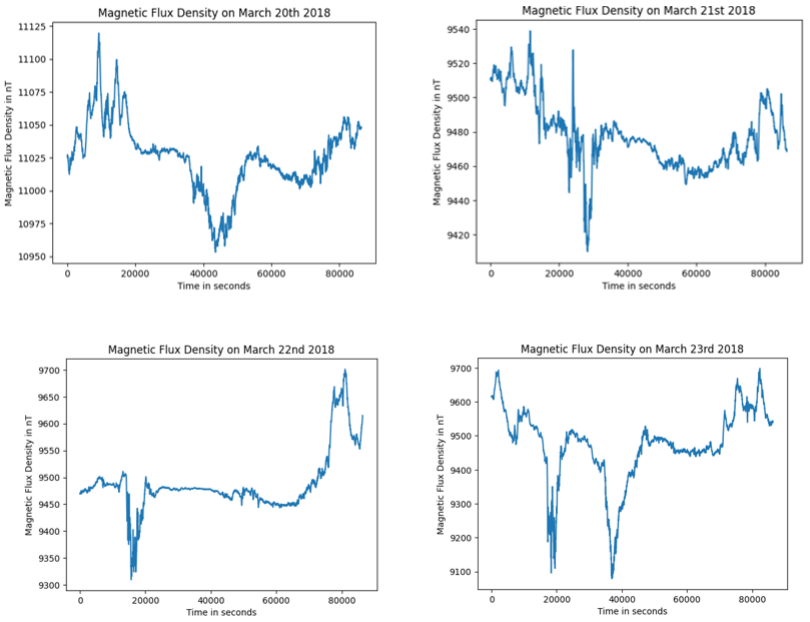

Fig. 3 Shows an example of the magnetic field from four days during the 2018 March event.

We use Fast Fourier Transformations (FFTs) to convert the raw magnetic field data provided by CARISMA and shown in Figure 3 into spectrograms for each day during the G1 storms, including the initial impact and recovery phase (See Figure 4).

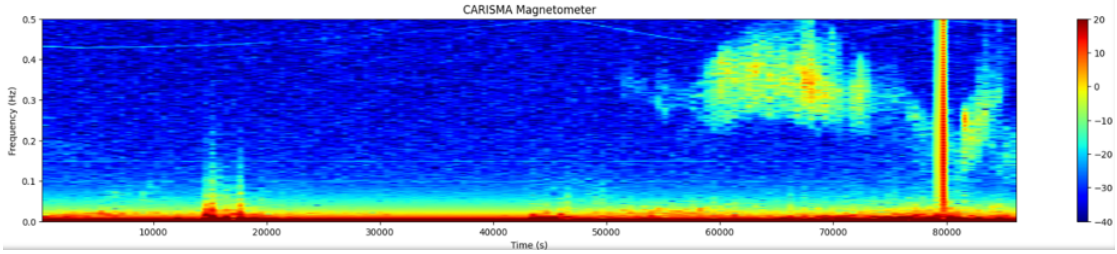

Fig. 4 Spectrogram of FSMI on March 22nd, 2018. The x-axis represents time in seconds, the y-axis represents frequency in Hz up to .5 Hz, and the colorbar represents relative power.

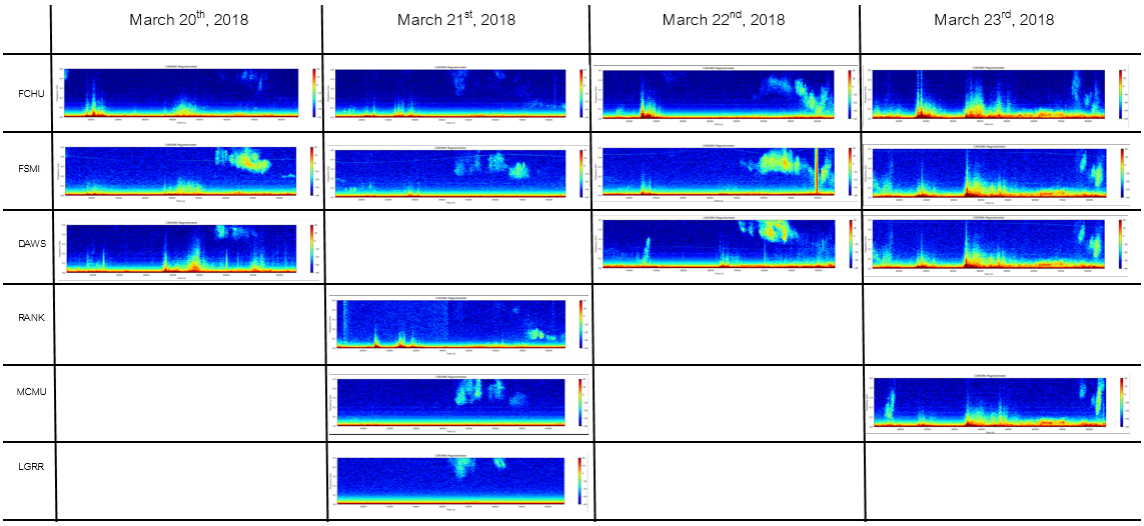

Fig. 5 Chart showing the spectrograms from 6 ground stations throughout the March 20th - 23rd event. Blank spaces represent a station that was not recording data or showed no activity.

Looking at Figure 5, we find when the waves are occurring in universal time (UT). We can use this to show that the waves occur in the same universal time (or similar) across multiple CARISMA stations on each day. In order to learn more about how the waves act in local time (LT), we converted the spectrograms to polar plots and shifted from UT to LT.

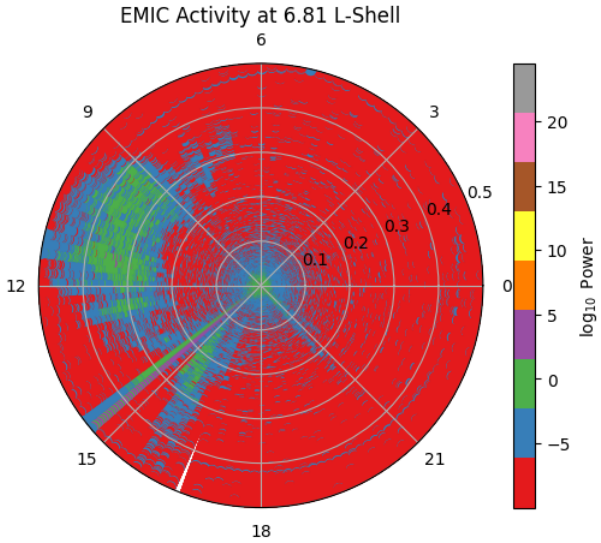

Fig. 6 Polar spectrogram from FSMI on March 22nd, 2018. Wave frequency is plotted on the radial axis, and azimuth shows LT.

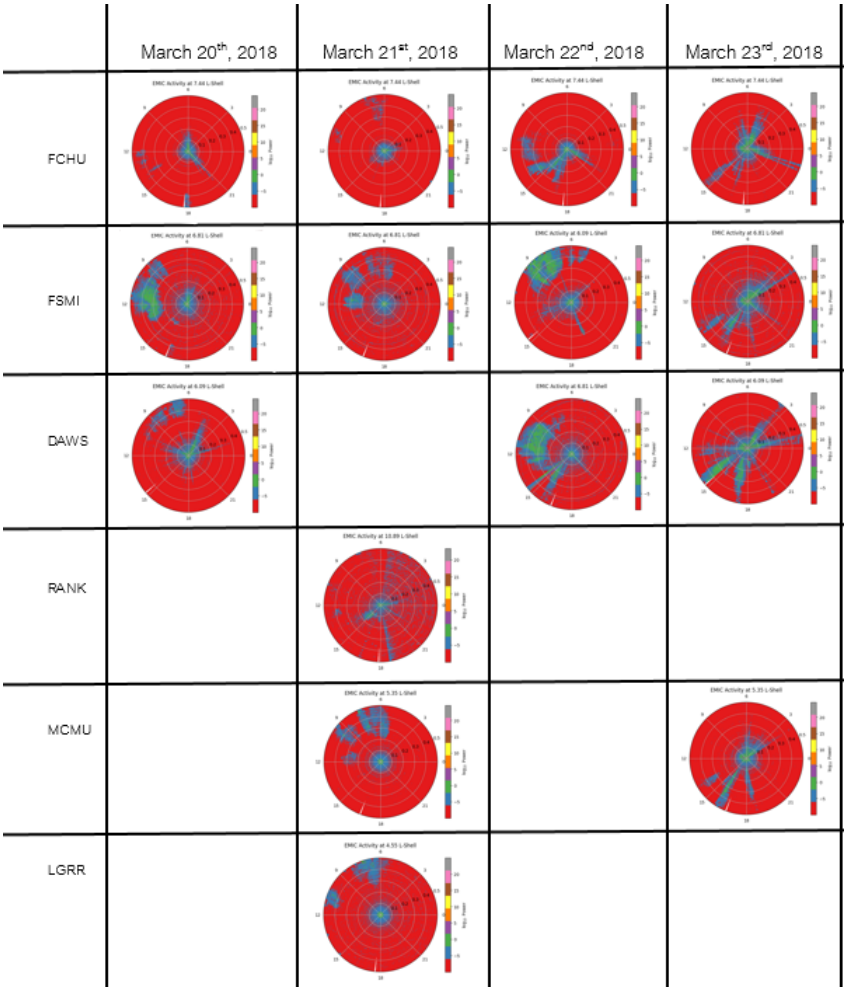

Fig. 7 Chart showing polar spectrograms for each CARISMA ground station. Plots are oriented so that the Sun is to the left and local noon or 12LT. Blank spaces represent a station that was not recording data or showed no activity.

Converting the spectrograms to polar coordinates allows us to put the location of the waves in perspective with the location of Earth relative to the Sun. The plots in Figure 7 show us that the majority of these waves occur on the dayside of the magnetosphere and toward the end of the event we observe that the waves are shorter in duration and less powerful. Once we could document where the waves occurred, we could begin to create a picture of how these waves behaved over the course of each event.

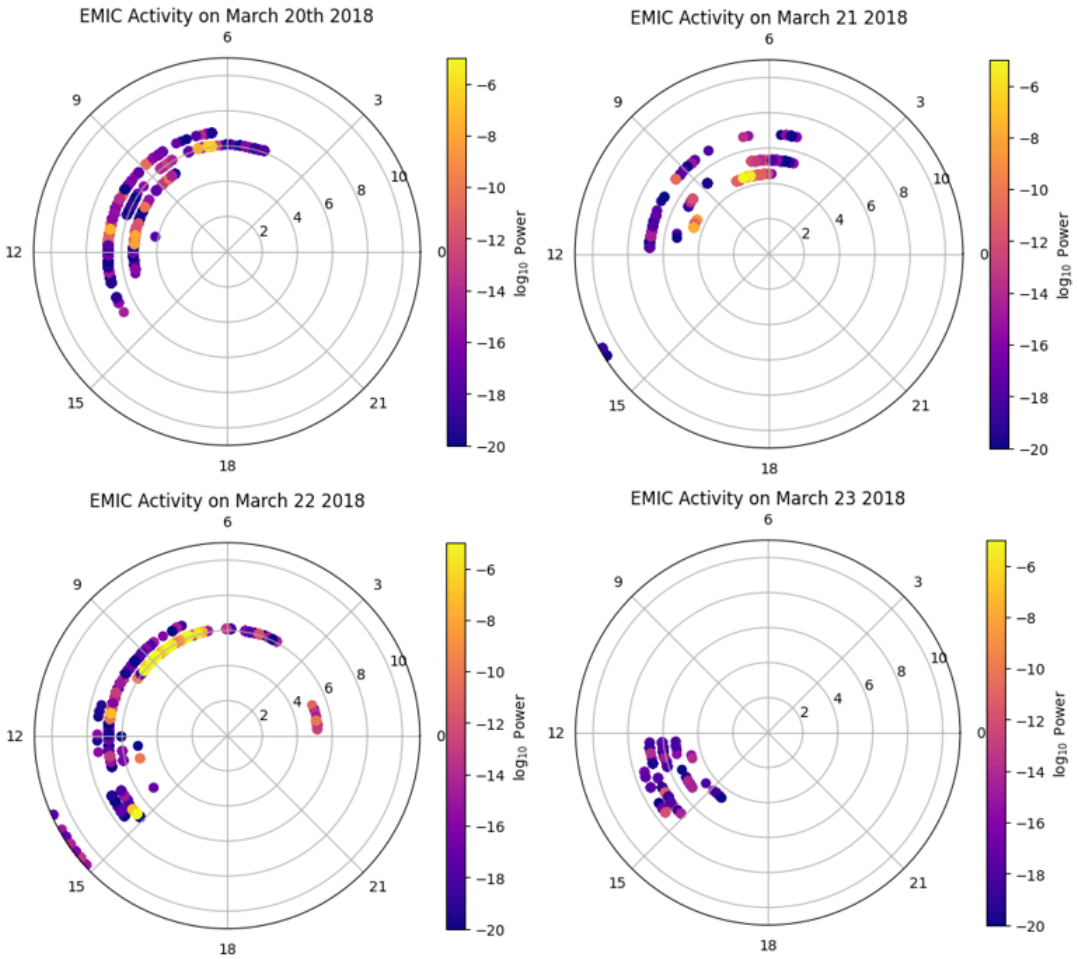

Fig. 8 Plots of EMIC mapping across March 2018 event in which radius represents L-shell and azimuth represents LT.

We filtered the polar spectrograms to only show the wave activity in LT, compared along side multiple CARISMA ground stations located at different L-shell to get a complete map of EMIC wave activity on each day. L-shell describes the distance away from Earth at the magnetic equator, where L is in units of Earth radii. L-shell is estimated for each ground station by taking its location and mapping along Earth's magnetic field out to the equatorial plane. The higher in latitude a magnetometer is located on Earth, the farther L-shell it will record at. The plots in Figure 8 are showing that the waves have a slight shift toward nightside as the event progresses, but mostly is contained to the dayside. We see this in from the plot of March 20th, 2018 where the waves are contained between about 6 LT and 12.5 LT, and the plot of March 23rd, 2018 where the waves are contained to after 12 LT. These again show a decrease in relative power as that shift toward the nightside occurs and during the recovery of the G1 storm.

III. Observations

Seeing these waves activate across the magnetosphere created questions about drivers for such wave activity. In particular, we aim to determine whether these waves are turning on and off each day of the March event, or persisting multiple days as ground stations rotate into and out of the wave region on the dayside. To get a better understanding of the solar wind and geomagnetic conditions during the EMIC events, we examined the OMNI data below. EMIC waves have a dependance on the generation mechanism, so exploring solar wind speed, proton density and the SYM/H plots available from OMNI, allows us to examine why and how these waves may be occurring. SYM/H is the baseline-corrected, magnetic longitude-adjusted average of the disturbance of the magnetic field, measured in nT; it is comparable to Dst. We performed a comparison of the OMNI data plots to the spectrograms of the CARISMA data. This allowed us to match up the increases in proton density, SYM/H, AE to EMIC generation.

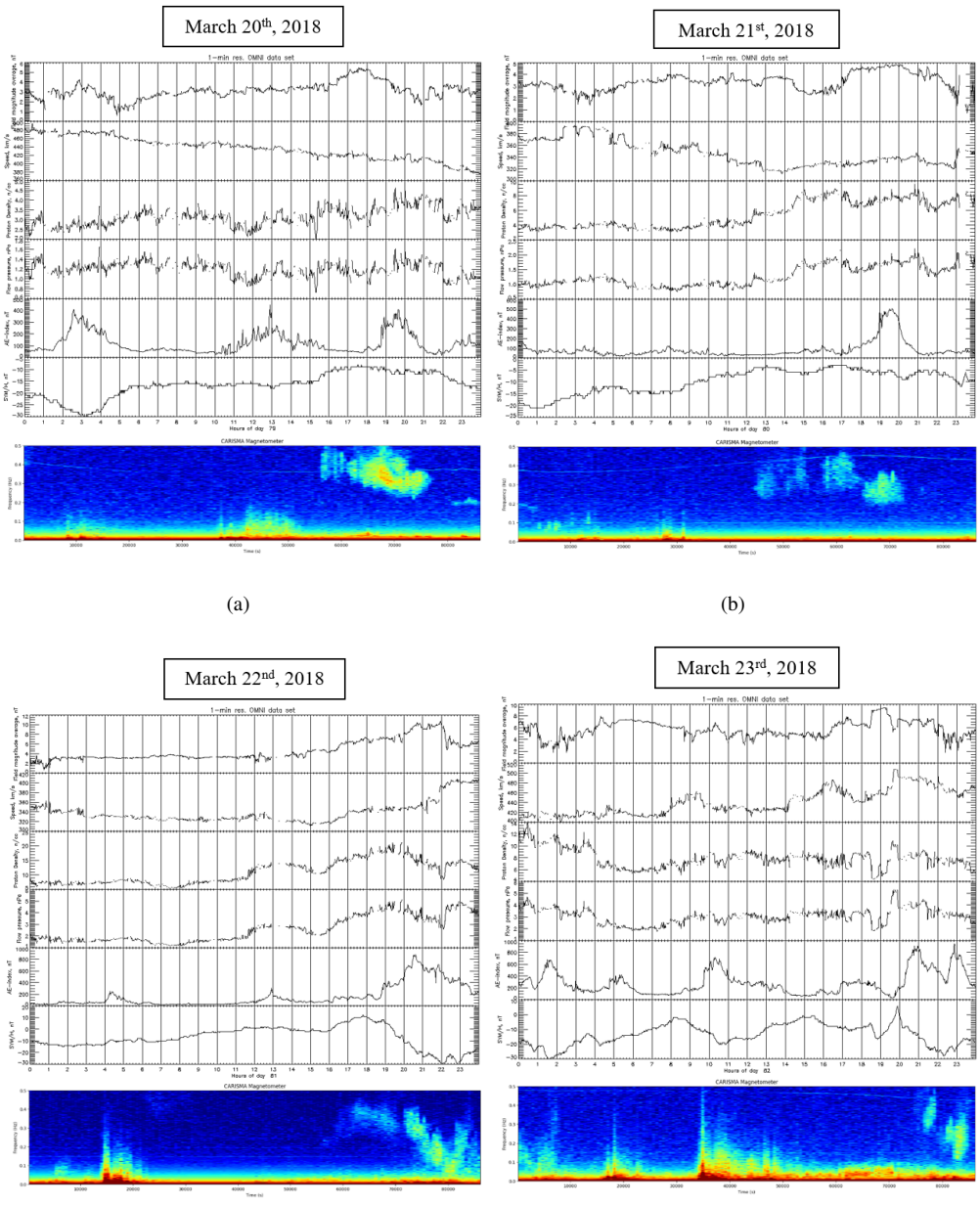

Fig. 9 Comparison of OMNI solar wind data (top 6 panels) to ground station spectrograms (bottom panel) during the March 2018 event. OMNI data includes magnetic field strength, solar wind speed, solar wind proton density, solar wind flow pressure, AE-index, and SYM/H.

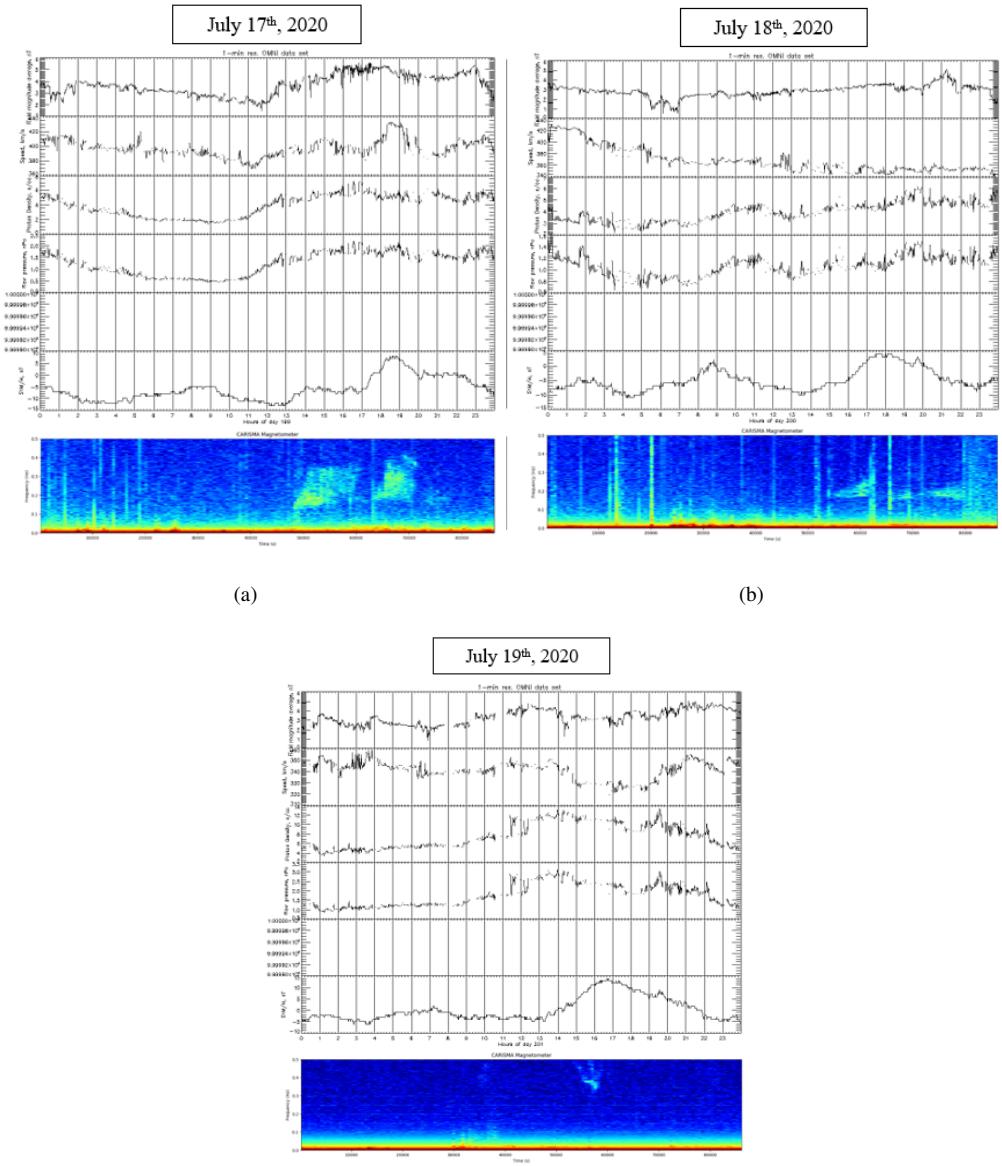

Fig. 10 Comparison of OMNI solar wind data (top 6 panels) to ground station spectrograms (bottom panel) during the July 2020 event. OMNI data includes magnetic field strength, solar wind speed, solar wind proton density, solar wind flow pressure, AE-index, and SYM/H. In this case, the AE-index was not recorded.

Figure 9 presents solar wind, geomagnetic activity, and EMIC wave activity during the March event. We see SYM/H dip down to $\leq |-30|$ nT on March 20th at approximately 03:00 UT and then follow into recovery. We see two other dips down to $\leq |-30|$ nT in SYM/H on March 21st at approximately 01:00 UT from March 22nd into March 23rd at approximately 23:00 UT on March 22nd. While solar wind pressure and speed vary throughout the four day period, there are no sharp or large changes that align with the start and stop of the EMIC waves on any of the days. The solar wind pressure varies from approximately 0 to 5 nPa.

Figure 10 presents similar data for another event that occurred in July 2020. Similar to the March event, we don't see any sharp or large changes in solar wind pressure or speed that align with the start and stop of the EMIC waves. The solar wind pressure varies from approximately 0 to 3.5 nPa.

Looking at this data we see an oscillatory behavior in the SYM/H and proton density plots. We see some matches in SYM/H with EMIC waves on March 22nd at approximately 21:00 UT and on March 23rd at approximately 21:00 UT. We also see a match in the July event on July 17th at approximately 17:00 UT and 19:00 UT. However, the SYM/H oscillations do not consistently align with each generated EMIC wave. There is only a correlation to some of the waves, thus it is inconclusive. On top of this, the AE plots show some correlation, but not enough to be conclusive. When looking at these plots, we fail to see any major driving force in the solar wind speed or proton density. Thus we see no obvious motivators from the OMNI-spectrogram comparison, suggesting there was not a clear solar driver and that internal magnetosphereic dynamics may have produced these waves instead.

With no clear solution from the OMNI-spectrogram comparison, we moved on to compare two different stations across Canada to better determine if the waves are turning on and off in time or persisting while ground stations rotate into and out of the wave region each day. We plotted the data from stations separated in longitude (and thus in local time) in Canada and compared the timing and location of waves observed by each station (see figures 11 and 12).

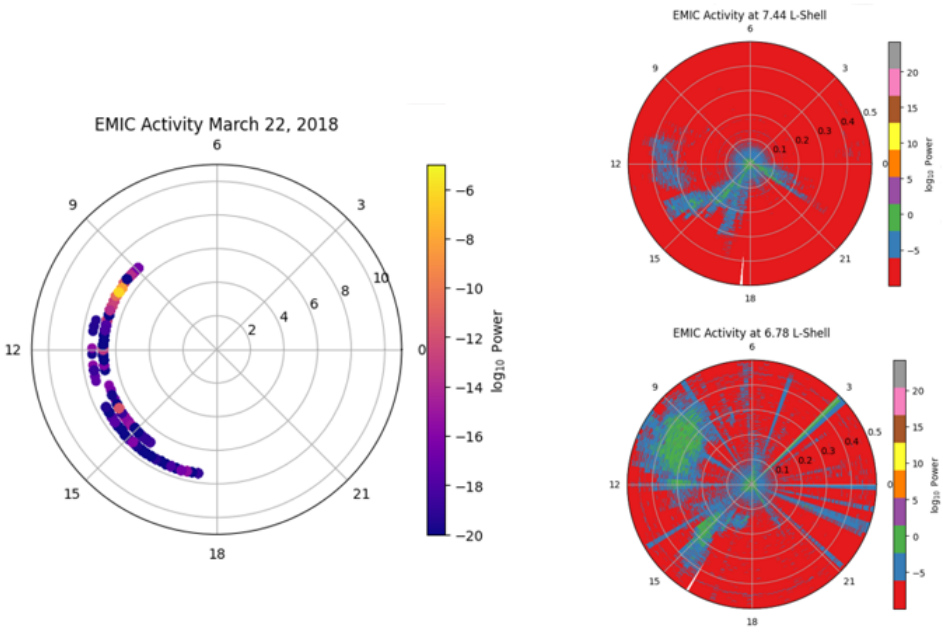

Fig. 11 Plots of EMIC mapping across March 22nd, 2018 in which radius represents L-shell and azimuth represents LT. Polar plots of FCHU (L of 7.44) and FSIM (L of 6.78) in which radius represents frequency and azimuth represents LT.

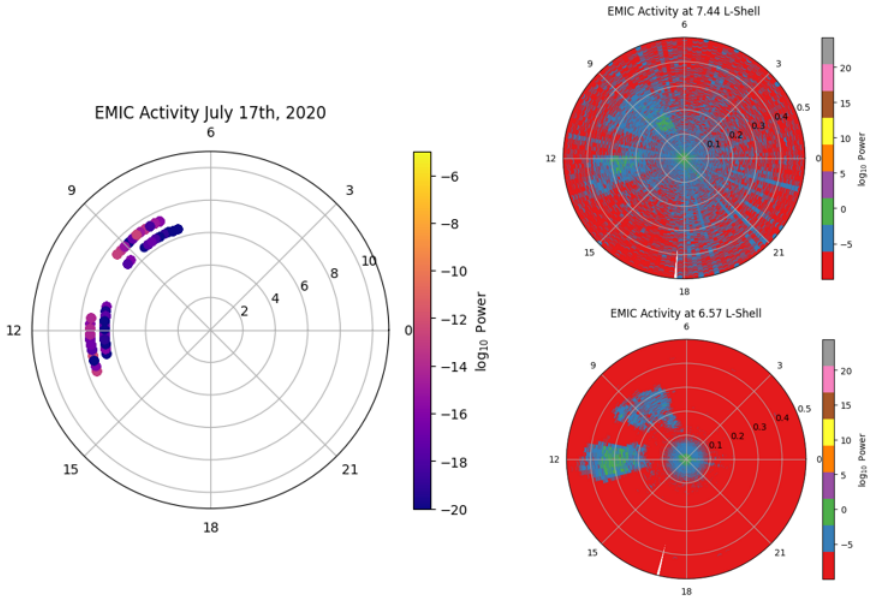

Fig. 12 Plots of EMIC mapping across July 17th, 2020 in which radius represents L-shell and azimuth represents LT.Polar plots of FCHU (L of 7.44) and RABB (L of 6.57) in which radius represents frequency and azimuth represents LT.

Looking at these plots, we see the separation in the time of which the waves are activated is proportional to the difference in LT of the stations. For example, with the station comparison on March 22nd, 2018, FCHU and FSIM have approximately a 1.81-hour difference between them, which is evident in the time difference between the wave generation we see on these mapping plots in Figure 11. We also observe with Figure 12 and FCHU and RABB during the July event, they have approximately a .64 hour difference in location and we see about that difference in the generation of their waves. These data suggest the waves turn on and off simultaneously across these locations, otherwise we would see the waves occurring at the location across the different stations.

IV. Discussion

In Figures 9 and 10, we see the OMNI data provides insights about the SYM/H during these events, without showing significant drivers in solar wind or proton density. This is in contrast to what has been observed in other studies of dayside EMIC waves, which often primarily show clear correlations between increases in solar wind pressure and EMIC wave onsets. (Usanova et. al., 2008, Engebretson et. al., 2002). Previously, long-duration EMIC waves have been observed and tend to occur in the recovery period after a geomagnetic storm, rather than from solar wind pressure pulses. However, these observations during the two events examined here show long-duration EMIC waves propagating on the dayside both without a clear solar wind driver. In Figures 9 and 10, we can see that there is no strong correlation between the OMNI data and the generation of the waves. We see some minor correlations between the AE and the wave

generation, however there is not great enough support for clear causation. Otherwise, we see no solar wind drivers that appear to be generating these long-duration waves.

In Figures 11 and 12, we compare two stations with different LT to confirm the duration of these waves. We see that the difference between the location of the waves in LT matches the difference between the stations in LT. This supports the idea that these waves are generated multiples times during the event, rather than lasting multiple days with the stations rotating in and out of the wave location.

Thus, we have found that these EMIC waves are occurring during G1 storms where they are repeatedly generated in almost a periodic fashion for multiple days during the recovery period of the storm. Without a clear generator of these waves, we have no clear cause for the wave existence. Further investigations into these waves could provide reasoning behind their creation and explain the duration and repeated generation.

In conclusion, we found that these waves are generated on the dayside, lasting for up to approximately eight hours a day and repeating for up to four days during the recovery period of a G1 storm. There are no clear solar wind compressions that are directly related to the generation of these waves and no other clear generator for such waves. Throughout this study, we investigated the events shown above as well as two other events in August 2016 and another in March 2018 that showed similar long-duration or repeated EMIC wave activity.

Moving forward, investigating further into the conditions of the magnetosphere and other possible drivers for these waves would provide further insight into the nature of these waves. Normally, long-duration EMIC waves have been seen on the nightside, while dayside waves are often short-lived and associated with compression from the solar wind. This discovery of long-duration EMIC waves on the dayside, without a clear driver could provide more information on the actions in our magnetosphere and wave generation within it. It would also be enlightening to further investigate the solar conditions for possible CIRs and whether there are any periodic structures that could contribute to such recurrent magnetospheric wave activity.

V. References

Anderson, B. J., and D. C. Hamilton (1993), Electromagnetic ion cyclotron waves stimulated by modest magnetospheric compressions, J. Geophys. Res., 98(A7), 11369–11382, doi:10.1029/93JA00605.

Blum, L., X. Li, and M. Denton (2015), Rapid MeV electron precipitation as observed by SAMPEX/HILT during high-speed stream-driven storms. J. Geophys. Res. Space Physics, 120, 3783–3794. doi: 10.1002/2014JA020633.

Blum, L. W., J. W. Bonnell, O. Agapitov, K. Paulson, and C. Kletzing (2017), EMIC wave scale size in the inner magnetosphere: Observations from the dual Van Allen Probes, Geophys. Res. Lett., 44, 1227–1233, doi:10.1002/2016GL072316.

Blum, L. W., Remya, B., Denton, M. H., and Schiller, Q. (2020). Persistent EMIC wave activity across the nightside inner magnetosphere. Geophysical Research Letters, 47, e2020GL087009. https://doi.org/10.1029/2020GL087009

Blum, L. W., Bruno, A., Capannolo, L., Ma, Q., Kataoka, R., Torii, S., and Baishev, D. (2024). On the spatial and temporal evolution of EMIC wave-driven relativistic electron precipitation: Magnetically conjugate observations from the Van Allen Probes and CALET. Geophysical Research Letters, 51, e2023GL107087. https://doi.org/10.1029/2023GL107087

Borovsky, J. E., and M. H. Denton (2006), Differences between CME-driven storms and CIR-driven storms, J. Geophys. Res., 111, A07S08, doi:10.1029/2005JA011447.

Engebretson, M. J., W. K. Peterson, J. L. Posch, M. R. Klatt, B. J. Anderson, C. T. Russell, H. J. Singer, R. L. Arnoldy, and H. Fukunishi, Observations of two types of Pc 1–2 pulsations in the outer dayside magnetosphere, J. Geophys. Res., 107(A12), 1451, doi:10.1029/2001JA000198, 2002.

Engebretson, M. J., Posch, J. L., Capman, N. S. S., Campuzano, N. G., Bělik, P., Allen, R. C., et al. (2018). MMS, Van Allen Probes, GOES 13, and ground-based magnetometer observations of EMIC wave events before, during, and after a modest interplanetary shock. Journal of Geophysical Research: Space Physics, 123, 8331–8357. https://doi.org/10.1029/2018JA025984

Kakad, A., Upadhyay, A., Kakadm B., and Rawat, R. (2023). Long-lasting Electromagnetic Ion Cyclotron wave signatures at Indian Antarctic Station, Maitri, Advances in Space Research, 71, https://doi.org/10.1016/j.asr.2022.08.021.

Ozeke, L. G., Mann, I. R., Dufresne, S. K. Y., Olifer, L., Morley, S. K., Claudepierre, S. G., et al. (2020). Rapid outer radiation belt flux dropouts and fast acceleration during the March 2015 and 2013 storms: The role of ULF wave transport from a dynamic outer boundary. Journal of Geophysical Research: Space Physics, 125, e2019JA027179. https://doi.org/10.1029/2019JA027179

Usanova, M.E., Mann, I.R. and Darrouzet, F. (2016). EMIC Waves in the Inner Magnetosphere. In Low-Frequency Waves in Space Plasmas (eds A. Keiling, D.-H. Lee and V. Nakariakov). https://doi.org/10.1002/9781119055006.ch5

Usanova, M. E., I. R. Mann, I. J. Rae, Z. C. Kale, V. Angelopoulos, J. W. Bonnell, K.-H. Glassmeier, H. U. Auster, and H. J. Singer (2008), Multipoint observations of magnetospheric compression-related EMIC Pc1 waves by THEMIS and CARISMA, Geophys. Res. Lett., 35, L17S25, doi:10.1029/2008GL034458.

Wang, D., Z. Yuan, X. Yu, X. Deng, M. Zhou, S. Huang, H. Li, Z. Wang, Z. Qiao, C. A. Kletzing, and J. R. Wygant (2015), Statistical characteristics of EMIC waves: Van Allen Probe observations. J. Geophys. Res. Space Physics, 120, 4400–4408. doi: 10.1002/2015JA021089.

Williams, D.J. Dynamics of the earth's ring current: Theory and observation. Space Sci Rev 42, 375–396 (1985). https://doi.org/10.1007/BF00214994